Macromolecules

ARTICLE

pubs.acs.org/Macromolecules

Full Characterization of PB−PEO Wormlike Micelles at Varying Solvent Selectivity

B. Lonetti,*[,†,§] A. Tsigkri,[†] P. R. Lang,[†] J. Stellbrink,[†] L. Willner,[†] J. Kohlbrecher,[‡] and M. P. Lettinga[†]

[†]Institut für Festkörperforschung, Forschungszentrum Jülich, D-52425 Jülich, Germany

[‡]Laboratory for Neutron Scattering, ETH Zürich and Paul Scherrer Institut, 5232 Villigen PSI, Switzerland

ABSTRACT: Poly(butadiene−ethylene oxide) (PB−PEO) block copolymers form wormlike micelles in water. These structures can be characterized over a very broad range of length scales, ranging from the contour and persistence length to the core/corona diameter and the total aggregation number. Here we use fluorescence microscopy, dynamic and static light scattering and small angle neutron scattering to obtain information on the full range of length scales, while changing the solvent selectivity of the block copolymer by varying the molar ratio of mixtures of *N*,*N*-dimethylformamide (DMF) and water. We show that the wormlike micelles become very small and flexible before a transition to spherical micelles sets in decreasing the interfacial tension. We calculated the free energy contributions for the different species using the experimental input and confirmed that the transition to spherical micelles is energetically favored.

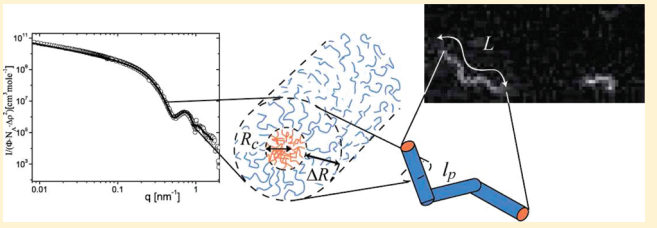

INTRODUCTION

In the last few years, the self-assembly of block copolymers has been a subject of great interest, thanks to the variety and robustness of the structures they form in selective solvents.[1−3] Extensive studies demonstrated that the micellar morphology can be tuned (going from spheres, cylinders, worms, and vesicles) by varying the block copolymer molecular weight, the chemical nature, and the ratio of the blocks.[4−7] One of the most extensively studied block copolymers is poly(butadiene−ethylene oxide) (PB−PEO). As a function of the hydrophilic block length (in term of PEO weight fraction w_{PEO}) spherical micelles (w_{PEO} >0.6), wormlike micelles, WLM ($0.47 \leq w_{PEO} \leq 0.59$), or bilayers ($w_{PEO} < 0.47$) are formed.[6,7] The wormlike micelles persistence length as a function of core diameter revealed fluid objects following the stiffness scaling relation $l_p \sim d^3$,[8] where l_p is the persistence length and d is the core diameter of the wormlike particles. Finally, the lyotropic phase behavior of PB−PEO aggregates has been studied for total degree of polymerizations ranging from 118 to 1690 monomer units.[9]

Different theoretical studies contributed to define the scaling laws for the parameters of equilibrium structures.[10,11] Among them, a quantitative theory defining the thermodynamic stability of different morphologies in selective solvents has been recently developed.[12] The theory expresses the free energy contributions of the core, the corona, and the interface as a function of the blocks structural parameters and the interfacial tension between the solvent and the insoluble block for different micellar morphologies. It has been validated experimentally in the case of PS−PI in heptane.[12]

Solvent selectivity can be more easily tuned than the above-mentioned parameters (molecular weight, block ratio etc.) and moreover in a continuous way by varying the solvent composition. Therefore, solvent composition is a very natural and easy parameter to control the micellar structures.[13−18]

There are different approaches to tune solvent selectivity, leading to different transitions. Some polystyrene block copolymers have been dissolved in a common solvent, dioxane or DMF, and a selective solvent for the hydrophilic block has been added in order to form micelles. In the case of poly(stryrene-*b*-acrylic acid) (PS−PAA) in dioxane/water and *N*,*N*-dimethylformamide (DMF)/water mixtures, a morphological transition from spheres to vesicles was observed.[19] In DMF/water or DMF/acetonitrile mixtures, poly(styrene-ethylene oxide) (PS−PEO) micelles passed from spheres to worms to vesicles.[14] Similarly, poly(styrene-*b*-isoprene) (PS−PI) micelles in mixtures of different dialkyl phthalates, styrene selective solvents, changed from spheres to cylinders to vesicles.[13]

For all these examples, the change in the morphology of the self-assembled structures can be attributed to a change of solvent selectivity, which influences the different energy contributions responsible for the morphology: core−chain stretching, corona−chain repulsion, and interfacial tension between the core and the solution.

In this paper, we quantitatively study the effect of solvent selectivity on the micellar morphology of symmetric PB−PEO block copolymers. Parameters obtained from experiments are used as input for a recently developed theoretical approach to predict morphological transitions. We seek to have a complete understanding on all relevant length scales of the free energy that governs the structure of these self-assembled systems.

The interest is to relate changes on the smallest relevant length scale, i.e., diameter and aggregation number per unit length, to changes in the macroscopic structure, i.e., the contour and persistence length of the wormlike micelles and the transition from wormlike to spherical micelles. This molecular level understanding can help to elucidate the mechanisms involved in non equilibrium conditions.[20] Besides, it is expected that these quantities have a pronounced effect on the rheological behavior of the systems, and as such solvent composition could be used to tune the rheology.[15,21]

Received: November 19, 2010
Revised: April 1, 2011
Published: April 13, 2011

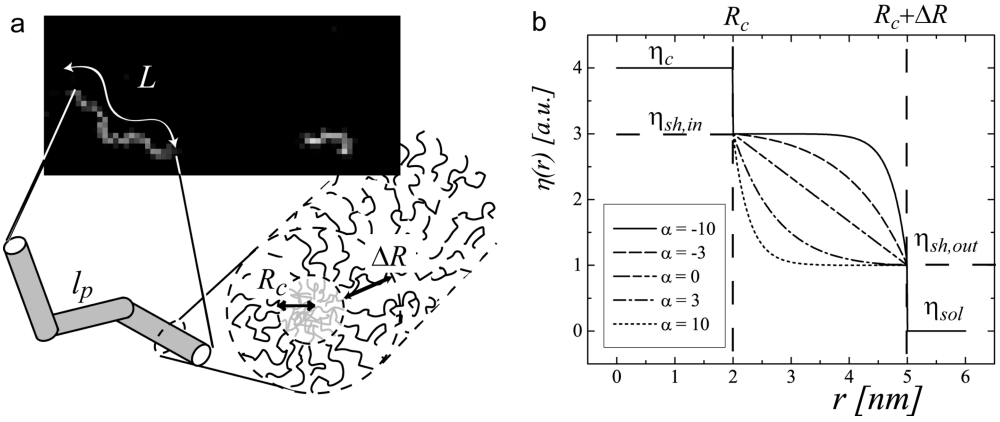

Figure 1. (a) Fluorescence microscopy image of one of the longest PB−PEO wormlike micelles. L is the worm's contour length and l_p its persistence length. The cross-section of the micelle is characterized by the shell thickness ΔR and the core radius R_c. The dashed line indicates the interface between the two block copolymers. (b) Exponential profile of the shell scattering length density. α is a parameter of the exponential shell profile (eq 9).

In order to probe these very different length scales, we need to use several complementary techniques to fully characterize the micelles in the range of the used experimental conditions. We use fluorescence microscopy to determine the tail of the contour length distribution and the persistence length. We use dynamic light scattering (DLS) to determine the length polydispersity and static light scattering (SLS) to determine the persistence length. Especially SLS is useful at high DMF contents since then the particles are too small to be characterized under the microscope. The core diameter and aggregation number per unit length are determined with small angle neutron scattering (SANS). All techniques are introduced in the experimental part, together with the used materials and synthesis, while in the Data Analysis section we show how the required parameters are extracted from the measurements. In the Results, we present the effect of the solvent selectivity on all different length scales, ranging from contour length to core diameter. In the Discussion, we show how all contributions to the micellar free energy can be derived with the input of the above-mentioned techniques and with the measurements of the interfacial tension of PB as a function of solvent composition by pendant drop tensiometry. Thus, we predict the transition from wormlike to spherical micelles, which we experimentally confirm.

EXPERIMENTAL PART

Material. In this study, we used a symmetric PB−PEO block copolymer prepared by living anionic polymerization following a two-step procedure; details can be found in an earlier publication.[22]

Size exclusion chromatography (SEC) was used for the block copolymer characterization. A mixture of tetrahydrofuran/dimethylacetamide 90/10 v/v was chosen as eluant. The polydispersity, M_w/M_n, of the block copolymer was smaller than 1.04. According to SEC chromatograms we can exclude the presence of PEO and PB homopolymers. Absolute molecular weights were determined by ^{1}H NMR measurements in $CDCl_3$ by taking the signal of the *tert*-butyl initiator group as an internal reference. The number-average molecular weights, M_n, are 2.60 kg mol^{-1} for PB and 2.64 kg mol^{-1} for PEO.

Deuterated solvents were used for preparing solutions: D_2O (Chemotrade, % D = 99.8%) and *N*,*N*-dimethylformamide-d_7, *d*-DMF (Chemotrade, % D = 99.5%). In order to guarantee a good homogenization in solution, polymer was dissolved in the solvent and kept for half an hour at 56 °C and then left to cool down slowly to the ambient temperature. The solvent composition will be expressed as DMF mole fraction, *f*.

The synthesized PB−PEO block copolymer self-assembles in water into long wormlike micelles (WLM)[6] where the PEO block constitutes the hydrophilic corona and the PB block the core, see Figure 1a. The interactions parameters' values $\chi_{PB\text{-water}} \approx 3.5$ and $\chi_{PB-PEO} \approx 0.4$[7] allow us to reasonably assume that the PB chains are highly segregated in the core, where neither water nor PEO chains can access.

Fluorescence microscopy images were taken with Hamamatsu C9100 EM-CCD camera (exposure time 10 ms) on a Zeiss Axioplan 2 microscope using a 40× oil, NA 1.0 objective.

We performed measurements of the micelles in different water/DMF solvent mixtures (0, 0.025, and 0.06 DMF mole fraction, *f*) at ambient temperature. The samples were prepared at the concentration of 0.5 wt %, far away from the isotropic/nematic transition 1.7%,[6,21] and the micelles were labeled with PKH67 (Sigma-Aldrich, excitation at 490 nm and emission at 504 nm) at a ratio of 1:1000. Then 5 μL of the solution were poured into a quasi 2-dimensional chamber formed by a microscope glass slide and a coverslip. In order to prevent the sticking of the micelles on the glass surface, both glass surfaces were coated with agarose by dipping the glass in a 0.3 mg/mL solution and sequential drying.

For the image processing, we used an IDL program provided by E. Barry.[23] After thresholding and skeletonization, each micelle contour longer than 4 pixels was selected. From every image we obtained a distribution of contour lengths and for enhancing our statistics about 50 images were obtained for each solvent mixture. If stacks of images (short movies) are recorded instead of single images, we can directly observe the thermal motion of the individual wormlike micelles and obtain information about their persistence lengths by analysis of the shape fluctuations.

Small angle neutron scattering data were collected at the SANS I instrument at the SINQ spallation source at the Paul Scherrer Institute (PSI) in Villigen, Switzerland.[24]

We used thermal neutrons of wavelength $\lambda = 0.7$ nm with a wavelength spread $\Delta\lambda/\lambda$ of about 0.1. We performed experiments at ambient temperature and at three different sample to detector distances (2, 6, and 18 m) to cover a range of scattering vectors from 0.02 to 3 nm^{-1} after radial averaging. When lenses were added at 18 m distance the scattering vector range was extended to 0.004 nm^{-1}.[25,26]

The data reduction was performed using the BerSANS software package (Keiderling 2002). Water was used as standard sample for absolute calibration of scattering intensities and for correction of nonuniform detector efficiency.

Polymer solutions were measured in quartz cells with a path length of 2 mm; the circular sample aperture was 16 mm. In the series of experiments the polymer concentration was kept constant at 0.5 wt % and the solvent composition was varied from pure D_2O to pure *d*-DMF (0, 0.026, 0.09, 0.2, 0.36, 0.5, 0.7, and 1 DMF mole fraction, *f*).

Interfacial tension measurements were performed at ambient temperature with the axisymmetric drop shape analysis technique using a commercial pendant drop tensiometer G10 from Krüss (Germany). The interfacial tension (γ) was calculated from the drop profile. Drop images were taken and analyzed every 5 s. The measurements lasted 2−3 hours, when the interfacial tension reached an asymptotic plateau value. The interfacial tension values are the average of three independent measurements of the plateau value. The PB1.4k polymer used for measurements is a low molecular weight (1.4 kDa) homopolymer prepared in the same way as the PB in the block copolymer.

Mass density of the PB1.4k and solvent mixtures, necessary for the determination of the interfacial tension was measured with an oscillation U-tube densitometer, DMA 5000 from Anton Paar. The measurement precision, as given by constructor, is 10^{-5} g/cm^3.

Light Scattering Experiments. Static and dynamic light scattering experiments were performed on an ALV/CGS-8F S/N 060 laser goniometer system (ALV, Langen, Germany), using a 22 mW He−Ne laser (λ = 633 nm) (JDS Uniphase, Milpitas USA) and a single avalanche photodiode detector. Compared to SANS we could reduce the concentration to 0.02 wt % of polymer dissolved in different D_2O/d-DMF solvent mixtures (*f* = 0, 0.026, 0.06, 0.09, 0.2, 0.26, 0.36, and 0.6).

For **static experiments** solvent mixtures of different DMF content were also prepared in order to take the solvent intensity as background. Scattering intensities were recorded in a range of scattering angles $13 \le \theta \le 150$ with an angular step of 1°, which corresponds to a range of scattering vectors $q = 4\pi n/\lambda[\sin(\theta/2)]$ varying with the index of refraction, *n*, and then corrected for the Rayleigh ratio of toluene (q_{min} = 0.003 q_{max} = 0.025 nm^{-1}).

In dynamic experiments the scattering angle varied from 13°-21° with an angular step of 2 and then intensities were measured at angles of 30°, 45°, 60°, 90°, and 120°.

Static and dynamic measurements were performed at ambient temperature.

DATA ANALYSIS

Model for the Form Factor from SANS and SLS. *Wormlike Micelles.* The form factor scattering function for wormlike micelles (WLM) of contour length L, $P(q,L,l_p)$, can be written as the product of the cross-section scattering, $P_{cs}(q)$, and the scattering from the conformation of the worm, $P_w(q,L,l_p)$, as the diameter of the worms is much smaller than the persistence length l_p[27,28]

$$P(q,L,l_p) = P_{cs}(q)P_w(q,L,l_p) \quad (1)$$

The data at low DMF content show a scattering behavior like from very long rods, $\sim q^{-1}$, independent of the micellar length, polydispersity and flexibility. Therefore, the conformation contribution $P_w(q,L,l_p)$ reduces to $P_w(q,L)$ and can be well approximated by the scattering of a very long thin rod whose length *L* is fixed to a large enough value

$$P_w(q,L) = \left(\frac{2}{qL}\mathrm{Si}(qL) - \frac{\sin(qL/2)}{qL/2}\right) \quad (2)$$

where $Si(x) = \int_0^x((\sin t)/(t))\,dt$ is the sinus integral.

For samples at higher DMF content the conformation contribution $P_w(q,L,l_p)$ of the worm has been described by the model from Kholodenko[29]

$$P_w(q,L,l_p) = \frac{2l_p}{3L}\left[I_{(1)}\left(\frac{3L}{l_p}\right) - \frac{l_p}{3L}I_{(2)}\left(\frac{3L}{l_p}\right)\right] \quad (3)$$

$$I_n(x) = \int_0^x f(z)z^{n-1}\,dz \quad (4)$$

$$f(z) = \begin{cases} \frac{1}{E}\frac{\sinh(Ez)}{\sinh(z)} & \text{for } q \le \frac{3}{l_pF}1\frac{\sin(Fz)}{\sinh(z)} \text{ for } q > \frac{3}{l_p} \end{cases} \quad (5)$$

$$E = \sqrt{1 - \left(\frac{l_pq}{3}\right)^2} \quad (6)$$

$$F = \sqrt{\left(\frac{l_pq}{3}\right)^2 - 1} \quad (7)$$

whereby *L* here describes the contour length of the wormlike micelle.

For the cross-section contribution, $P_{cs}(q)$, a radial profile, $\eta(r)$, with a homogeneous core and an exponential shell has been used:[30]

$$\eta(r) = \begin{cases} \eta_c & r \le R_c \\ \eta_{exp}\left(\frac{r-R_c}{\Delta R}\right) & R_c < r < R_c + \Delta R \\ \eta_{sol} & r \ge R_c + \Delta R \end{cases} \quad (8)$$

The exponential profile of the shell was described by

$$\eta_{exp}(x) = \begin{cases} \eta_{sh,in} + [\eta_{sh,out} - \eta_{sh,in}]x\exp([1-x]\alpha) & \alpha < 0 \\ \eta_{sh,out} + [\eta_{sh,in} - \eta_{sh,out}][1-x]\exp(-x\alpha) & \alpha \ge 0 \end{cases} \quad (9)$$

With $x = (r - R_C)/\Delta R$, R_c and ΔR the core radius and the shell thickness of the micelle, respectively; $\eta_{sh,in}$ and $\eta_{sh,out}$ are the values of the shell scattering length density at R_c and at $R_c + \Delta R$, respectively. This is a versatile model function where a single parameter α can describe all cases between slight penetration of the solvent into the shell ($\alpha < 0$) and a profile where the solvent strongly penetrates into the shell ($\alpha > 0$), via a linear decaying scattering length density profile ($\alpha = 0$) (see Figure 1b).

The scattering intensity for the radial symmetric scattering length density profile $\eta(r)$ is numerically calculated. The scattering amplitudes from the core, F_c, and the shell, F_{sh}, are given by:

$$F_C(q,R_C) = 2\frac{J_1(qR_C)}{qR_C} \quad (10)$$

$$F_{sh}(q,R_C,\Delta R) = \frac{\int_{R_C}^{R_C+\Delta R} 2\pi r J_0(qr)(\eta(r)-\eta_{sol})\,dr}{\int_{R_C}^{R_C+\Delta R} 2\pi r(\eta(r)-\eta_{sol})\,dr} \quad (11)$$

J_n are the Bessel functions of first kind with $n = 0$ and 1. The overall scattering intensity is than given by[31]

$$\begin{aligned} P_{cs}(q) &= N_{agg}^2\beta_c^2F_c^2(qR_C) + N_{agg}(N_{agg}-1)\beta_{sh}^2F_{sh}^2(q,R_C,\Delta R) \\ &+ 2N_{agg}^2\beta_c\beta_{sh}F_c(qR_C)F_{sh}(q,R_C,\Delta R) \\ &+ N_{agg}\beta_{sh}^2P_{local}(q,\Delta R) \end{aligned} \quad (12)$$

N_{agg} is the aggregation number of the worm which can be calculated from fitting the aggregation number per unit length n_{agg} (number of copolymer molecules per PB-core length of the worm), by $N_{agg} = n_{agg}L$. The last term in eq 12, describing the scattering of the individual PEO block, has for cylindrical geometries only a negligible contribution to the intensity as it only depends linearly on the aggregation number.

The excess scattering lengths of the core, β_c, and the shell, β_{sh}, are calculated from the scattering length densities of the PB (η_c) and PEO (η_{sh}) block of the copolymer, their molecular volumes (V_c and V_{sh}) and the scattering length density of the solvent (η_{sol}),

$$\begin{aligned} \beta_c &= V_c(\eta_c-\eta_{sol}) \\ \beta_{sh} &= V_{sh}(\eta_{sh}-\eta_{sol}) \end{aligned} \quad (13)$$

The scattering background of the individual PEO blocks has been described simply by the form factor of rods

$$P_{local}(q,\Delta R) = \left(\frac{2}{q\Delta R}\mathrm{Si}(q\Delta R) - \frac{\sin(q\Delta R/2)}{q\Delta R/2}\right) \quad (14)$$

However their contribution is almost negligible.

By the normalization via the excess scattering lengths β_c and β_{sh}, one accounts automatically for the fact that the core consists of pure PB and the shell of PEO plus solvent.

Using this parametrization, the relative scattering amplitudes of the shell and the core are the same as for the PB-block and PEO-block of a single copolymer, whose molecular weights and composition are well-known from the synthesis.

The input parameters for the model are the scattering length density of the solvent, the molecular volumes of the PB and PEO, V_c and V_{sh} together with their scattering length densities η_c and η_{sh}.

The fit parameters are the shell thickness ΔR, the shape parameter α of the scattering length density profile of the PEO shell, the aggregation number per unit length n_{agg}, the persistence length of the WLM, l_p, and the ratio of the scattering length density of the shell at the shell-solvent interface to the scattering length density at the core−shell interface, $r_0 = (\eta_{sh,out})/(\eta_{sh,in})$.

The aggregation number per unit length n_{agg} is assumed to have a log-normal distribution of width σ_{agg} and mode $n_{agg,0}$.

The core radius R_c can be computed by:

$$R_c = \sqrt{n_{agg}V_c/\pi} \quad (15)$$

Spherical Micelles. The scattering amplitudes we used in the case of spherical scatterers are the following:

$$F_c(q,R_c) = 3\frac{\sin(qr)-qr\cos(qr)}{(qr)^3} \quad (16)$$

$$F_{sh}(q,R_c,\Delta R) = \frac{\int_{R_c}^{R_c+\Delta R} 4\pi r^2\frac{\sin(qr)}{qr}(\eta(r)-\eta_{sol})\,dr}{\int_{R_c}^{R_c+\Delta R} 4\pi r^2(\eta(r)-\eta_{sol})\,dr} \quad (17)$$

The integrals for F_{sh} can be solved analytically. The overall scattering intensity is thus obtained from eq 12. For the form factor of spherical micelles the same radial scattering length density profile as defined in eq 8 has been used.

The fitting of the data was performed with the "SASfit" software package.[30]

Determination of the Average Contour Length and Polydispersity from Dynamic Light Scattering. The intensity autocorrelation function measured in DLS experiments, $g_2(q,t)$, is related to the normalized electric field autocorrelation function, $\hat{g}_1(q,t)$ through the Siegert relation $g_2(q,t) = 1 + A|\hat{g}_1(q,t)|^2$, where A is a prefactor accounting for instrumental imperfections.

Fluctuation of the scattered intensity for rod-like Brownian particles contains translational and rotational components and the electric field autocorrelation function is:[32]

$$\begin{aligned} \hat{g}_1(q,t,L,p) &= \sum_{n=0}^{\infty} S_{2n}(qL)\exp\{-[(C(qL)\Delta D + \overline{D})q^2 \\ &+ (4n^2+2n)D_r]t\} \end{aligned} \quad (18)$$

where D_r is the rotational (normal to the unit vector $\hat{u}$ describing the rod's orientation) diffusion coefficient and $\overline{D} = (2D_\perp + D_\parallel)/3$ is the average of the two translational diffusion coefficients $D_\parallel$ and $D_\perp$, parallel and perpendicular to the rods long axis. The term $C(qL)\Delta D$ accounts for the rotational translational coupling, where $\Delta D = k_BT[\ln p]/(4\pi\eta L)$, with, $p = L/d$, the rods' aspect ratio between the contour length, L, and the diameter, d, η is the solvent viscosity, and $C(qL)$ is inversely related to the rods' particle form factor.

The diffusion coefficients can be expressed in terms of the rods' length and aspect ratio[33]

$$\overline{D} = \frac{k_BT}{3\pi\eta L}(\ln p + 0.312 + 0.565p^{-1} - 0.10p^{-2}) \quad (19)$$

and

$$D_r = \frac{3k_BT}{\pi\eta L^3}(\ln p - 0.662 + 0.917p^{-1} - 0.050p^{-2}) \quad (20)$$

The coefficients S_{2n} are related to the particle scattering factor by

$$S_{2n}(q,L) = \frac{4n+1}{2}\frac{\left[\int_{-1}^{1} dx\, P_{2n}(x)j_0\left(\frac{L}{2}qx\right)\right]^2}{\int_{-1}^{1} dx\, {j_0}^2\left(\frac{L}{2}qx\right)} \quad (21)$$

where qx is the inner product of the scattering vector and the rods orientational unit vector, $P_{2n}(x)$ is the nth order Legendre

polynomial, j_0 refers to the spherical Bessel function of order zero, and the denominator represents the particle form factor.

To account for the length polydispersity of the micelles the expression for the correlation function has to be convolved with an appropriate distribution of micellar lengths. We tried different types of distribution functions and it turned out that the application of an exponential length distribution was most appropriate. Actually, when we fixed the micellar cross section diameter to the values obtained by SANS, we could not obtain reasonable fits to the experimental correlation functions using a Schulz−Zimm or a logarithmic normal distribution of the micelle lengths. Therefore, we used an exponential distribution

$$\Psi(L) = L \exp\left\{-\frac{L}{\mu}\right\} \tag{22}$$

as suggested by Dalhaimer et al.[34] For this frequency distribution, the mean value $\langle L \rangle \geq 2\mu$ and the standard deviation is given by $\sigma_L = (2)^{1/2}\mu$. With this the model function for the non linear least-squares fit of the experimental correlation function $g_2(t)$ takes the form

$$g_2(t) = 1 + A^2 \frac{\int_0^\infty \mathrm{d}L\ (L^2 P(Q)\hat{g}_1(L,p,q,t))^2 \Psi(L)}{\int_0^\infty \mathrm{d}L\ (L^2 P(Q))^2 \Psi(L)} \tag{23}$$

For each sample, five correlation functions, measured at different scattering angles, were fitted simultaneously, where μ was treated as a global parameter, while the amplitude A was allowed to float freely for each individual correlation function. In order to reduce computation time, the amplitudes S_{2n}, were calculated for $0 \leq n \leq 50$ as a function of discrete qL-values and stored in a look up table from which the values needed for the fitting were interpolated. The exemplary fits displayed in Figure 3 appear to be rather poor at first glance even for the situation where the micelles are dissolved in pure water. It has to be emphasized that individual correlation functions can be perfectly matched with the described model; however, the fits shown in Figure 3 were obtained with a simultaneous fit presuming a q^2-dependence of the relaxation rates, as implied by eq 18. However, the finite micelle flexibility causes a deviation from the q^2-dependence of the relaxation rates, as was shown by Song et al for monodisperse semiflexible rods,[35] which comes on top of the deviation caused by polydispersity. While the deviation due to polydispersity is covered by our model the effect of flexibility on the q-dependence of the relaxation rates is not captured.

Determination of the Persistence Length from Microscopy Data. The persistence length of wormlike micelles is directly related to the bending rigidity, which is obtained from the variance of the curvature fluctuations. After a skeletonization and a thinning procedure for every individual particle, we fit Gaussian profiles along cuts perpendicular to the particle contour for position refinement. Then the analysis of the shape fluctuations is done by use of Fourier decomposition. Having the exact pixel coordinates $(\chi_m y_m)$, we define the tangent angle θ as a function of the arclength s, which we then decompose into a sum of cosines:

$$\theta(s) = \sqrt{\frac{2}{L}} \sum_{n=0}^{\infty} a_q \cos(qs) \tag{24}$$

with $q = 2\pi n/\lambda$. The low modes contain information about the bending rigidity while the higher modes are dominated by experimental noise. In the long time limit, where the bending modes are decorrelated, the bending energy can be expressed as:

$$U = \frac{1}{2} k \int_0^L \left(\frac{\partial\theta}{\partial s} - \frac{\partial\theta_0}{\partial s}\right)^2 \mathrm{d}s \tag{25}$$

(wormlike chain Hamiltonian) where

$$\kappa = k_B T l_p \tag{26}$$

is the bending rigidity, with l_p the persistence length. By differentiation and integration of eq 25, we obtain the expression for the bending energy:

$$U = \frac{1}{2} k \sum_{n=1}^{\infty} q^2 (a_q^0 - a_q)^2 \tag{27}$$

By equipartition theorem, the saturating values of the mode amplitude fluctuations are

$$\langle (a_q(t+\Delta t) - a_q(t))^2 \rangle_{t,\Delta t \gg \tau} = \frac{2k_B T}{kq^2} \tag{28}$$

The persistence length is obtained by fitting the saturating mean-square amplitude versus q.[23]

RESULTS

Interfacial Tension. A measure of the solvent selectivity is given by the interaction parameter $\chi_{\text{PB-solvent}}$ between the insoluble block, PB and the solvent. The interaction parameter is directly proportional to the interfacial tension which goes from 37.2 ($f = 0$) to 4.4 mN m^{-1} ($f = 1$)[36]

$$\gamma = \frac{k_B T}{a^2}\left(\frac{\chi}{6}\right)^{1/2} \tag{29}$$

where k_B is the Boltzmann constant, T the temperature, χ the interaction parameter and a is the PB monomer length.

Figure 2 shows the decrease of the interfacial tension between PB1.4k and different solvent mixtures. Note that the solvent selectivity decreases with decreasing interfacial tension.

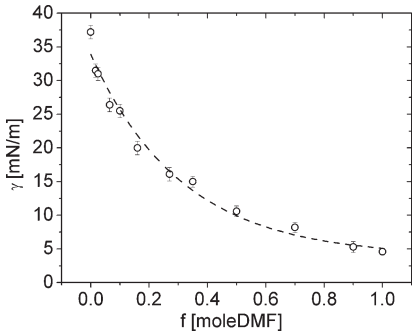

Figure 2. Interfacial tension, γ, of PB1.4k as a function of DMF mole fraction, f. The dashed line is an exponential curve $A + B \exp(-f/C)$, where $A = 3.9 \pm 0.6$, $B = 30.0 \pm 0.7$, and $C = 0.31 \pm 0.02$.

Contour and Persistence Lengths at Low DMF Content by Fluorescence Microscopy. Micelles labeled with a hydrophobic fluorophore (PKH67) were visualized by fluorescence microscopy. In Figure 3, we show the normalized distribution P of the contour lengths for the different solvent mixtures ($f = 0$, 0.025

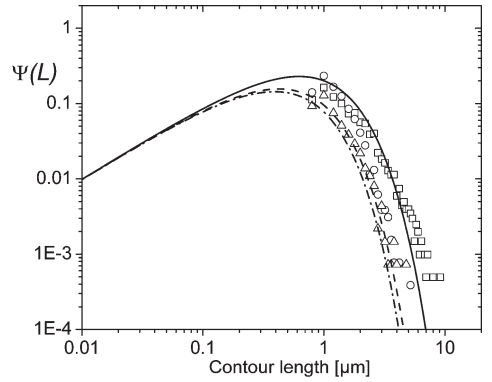

Figure 3. Probability density distribution of contour lengths for different molar fractions of DMF (solid line, square for $f = 0$; dashed line, circle for $f = 0.025$; dotted line, triangle for $f = 0.06$). The curves correspond to an exponential distribution with the parameters determined by DLS. The symbols are the data obtained from microscopy.

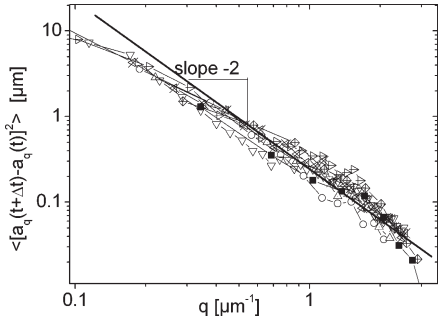

Figure 4. Mean- square amplitude values versus $q = 2\pi n/\lambda$ for pure water. The persistence length is calculated from the points that have slope −2, according to eqs 26 and 28. Here data from different individual particles are shown as different symbols in the graph.

and 0.06). At zero DMF we notice a long tail indicating the presence of particles with contour lengths of up to 10 μm. At $f =$ 0.025, the tail is far less extended and most of the particles have contour lengths between 1 and 2 μm. If the DMF content in the solvent is higher than $f = 0.06$, then the length of the WLM is too small to be resolved with the microscope and no reasonable statistics for contour length determination is feasible.

The analysis of stacks of images allowed us to directly observe the thermal motion of the individual WLMs and extract the persistence lengths by analysis of the shape fluctuations. Of course in order to have decent statistics a great number of particles is needed as well as observation over long time, which is difficult due to bleaching. Nonetheless, we were able to get a distribution of persistence lengths for a series of solvent mixtures, but since we are at the limit of the resolution, the data are noisy, leading to large error bars. According to eq 28, the fit of the saturating mean-square amplitudes as a function of q (see Figure 4) gives the persistence length.

The thus obtained persistence lengths for the three solvent mixtures are ∼1 μm (see inset in Figure 9) and within experimental error constant. In particular, for high DMF mole fraction, the error increases because the WLMs are smaller, and therefore the statistics of the thermal fluctuations from the image data is poor.

From microscopy measurements we can conclude that for WLMs in pure water there is a large variety in length reaching up to WLMs with a contour length of 10 μm. The length of the wormlike micelles decreases with increasing DMF content. The persistence length measurements are not conclusive due to their large error bars.

Dynamic Light Scattering. From microscopy, we obtained an estimate of the distribution of rod lengths especially in the high-L tail of the distribution for the long worms. The full distribution cannot be accessed because microscopy does not allow the determination of the length at the small side of the length distribution. Dynamic light scattering was used to obtain the average length and an estimate of the distribution width of the system.

Figure 5 reports the normalized correlation functions for $f = 0$, 0.06, and 0.2 for a few selected angles. They were fitted with the model function for rigid rods which takes into account the rotational and translational diffusion and their coupling, and the length polydispersity assuming an exponential distribution (eqs 18−23).

From the above fits we obtain information about the mean effective contour length ⟨L⟩ and the standard deviation of the length distribution of the rods σ_L. The quality of the fits is good at low f and becomes increasingly poor as f increases due to the increasing flexibility of the micelles with f. A quantitative criterion for the fit quality is the sum of squared deviations, χ^2, which is listed in Table 1 together with the best fitting parameter values. The unsatisfactory fits at increasing f can be attributed to the increasing flexibility which is not captured by the model function. We defined $\chi^2 > 10$ as a threshold above which the fits are too poor and the parameter values are not to be trusted anymore. Thus, as for the fluorescence microscopy, with DLS reliable results are only obtained at low f. The average contour lengths of <L> in the range of 0.8−1.2 μm which we find in the samples with low DMF concentration using DLS are in reasonable agreement with the contour lengths measured with fluorescence microscopy. With the latter technique the observed lengths were typically larger than 1 μm. Furthermore, if we calculate the entire distribution using the fitting parameters obtained from DLS, we find satisfactory agreement with the distributions measured with fluorescence microscopy. This is shown in Figure 3, where we plotted the distribution obtained from DLS together with the microscopy data. The underestimation of the lengths of the wormlike micelles in the high-L tail of the length distribution can possibly be explained by the fact that flexibility is not included in the fitting model. For high f this is a prerequisite. To our knowledge, the only analytical theory available for this problem is the fuzzy cylinder theory, which was originally proposed by Sato et al[37,38] and further developed by Einaga et al.[39,40] However, as Einaga points out, this theory is valid only for small scattering vectors or short cylinders, i.e., in the range $qL < 1$. Since in the present case we instead find $q\langle L\rangle \approx 10$ this theory is not applicable.

Small Angle Neutron Scattering and Static Light Scattering. Small angle neutron and light scattering allow us to characterize the micelles at smaller length scales than fluorescence microscopy. Figure 6 reports the absolute scattering cross section for a series of polymer solutions where the solvent changes from pure D_2O (DMF mole fraction, $f = 0$) to pure d- DMF (DMF mole fraction, $f = 1$).

In the case of high water content, at low q values, the scattering intensity follows a q^{-1} power law, typical for a cylindrical

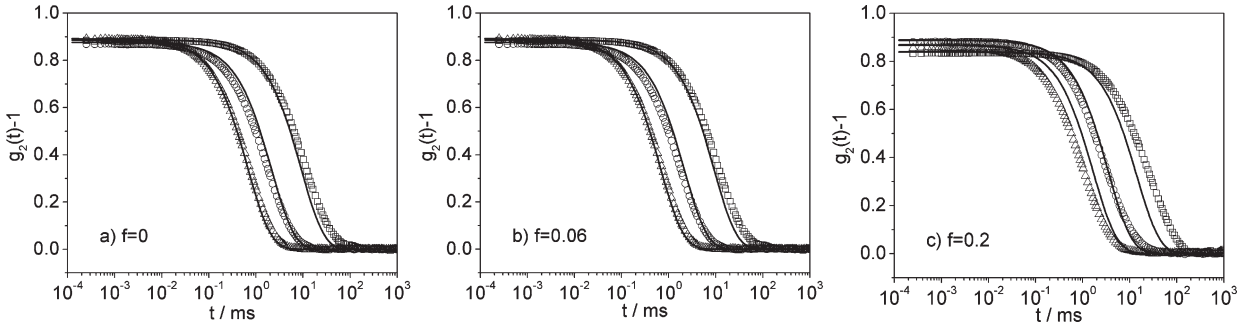

Figure 5. Correlation functions at different scattering angles (square = 30°, circle = 60°, and triangle = 90°) with fits assuming polydisperse rigid rods, for f = 0, 0.06, and 0.2. Symbols are experimental data and the full lines represent the best fits with the method described in the Experimental Part.

Table 1. Results from Fits of Dynamic Light Scattering Correlation Curves for Increasing DMF Content f[a]

f	d [nm]	μ [nm]	$\langle L\rangle$ [nm]	χ^2	σ_L [nm]
0	28.4	640	1280	3.64	905
0.026	28.7	425	850	3.61	600
0.06	27.9	390	780	5.0	550

[a] The parameter μ is related to the mean contour length by $\langle L\rangle = 2\mu$, and the standard deviation is given by $\sigma_L = (2)^{1/2}\mu$ The cross-sectional diameter, d, was fixed to the value obtained by SANS during the fitting. The sum of squared deviations χ^2 gives information about the quality of the fits.

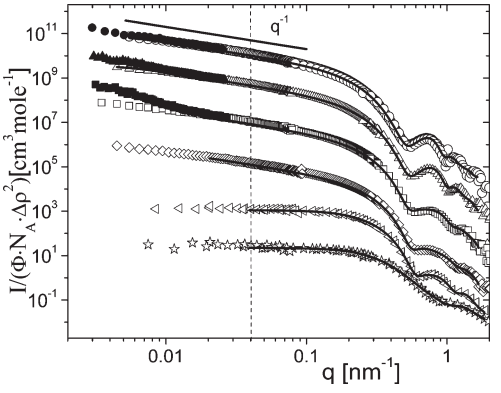

Figure 6. (a) Experimental (open symbols, SANS; filled symbols, SLS) and fitted (lines) scattering intensities as a function of the scattering vector for different solvent compositions going from d-DMF to D_2O (circle for f = 0, up triangle for f = 0.09, square for f = 0.36, diamond for f = 0.5, left triangle for f = 0.7, star for f = 1. The dashed line in the figure defines the range of fit of SANS data. In this q range the effect of possible micelles' interactions are negligible. For sake of clarity, data were shifted by arbitrary factors.

structure. No sign of the q^{-2} dependence, typical for wormlike micelles is observed: as the WLM's persistence length is bigger than 500 nm ([41] and our results), this zone falls outside the range accessible by our scattering experiments. Only the local cylindrical and more rigid structure can be accessed.

For f higher than 0.09, static light scattering measurements (filled symbols in Figure 6) show a change in the scattering vector dependence and allow us to obtain information on the WLM persistence length. This technique is complementary to SANS as it can access lower scattering vectors and lower polymer concentration. Although larger length scales can also be reached with SANS when using lenses, with SLS measurements the scattering intensity is much higher when using a laser. Thus, we can be sure to avoid any influence from the intermicellar interactions, using SLS concentrations that were a factor 10 lower than used for SANS. Fits of the SANS data in the whole q range using the Random phase Approximation indicated the influence of micellar interactions, the discussion of which is beyond the objective of this paper.

Looking at Figure 6, we can qualitatively observe a transition to spherical micelles. By adding DMF until f = 0.5, a 50% decrease in the scattering intensity is observed with no change in the slope. From f = 0.70 the q^{-1} dependence at low q is replaced by a plateau, indicating the presence of spherical objects. Also the minimum position in the form factor oscillations moves to higher q values, indicating smaller overall cylinder diameter with increasing DMF content.

In order to quantify this phenomenon, the scattering curves have been analyzed according to equations described in the Data Analysis section.

Over the entire cylinder region the shell radius ΔR, and the α parameter decrease with increasing DMF content as shown in Figure 7a; also the aggregation number per unit length n_{agg} decreases. As a result the core radius R_c decreases with increasing DMF content (eq 15 and Figure 7b). At the cylinder-to-sphere transition, a jump of ΔR and R_c is observed.

Figure 8 shows the SLS scattering data normalized by the polymer concentration in the so-called Holtzer representation (Iq vs q) which highlights the region with the scaling power −1 typical of cylindrical structures. A plateau is present at low DMF content; while a slope change is present at higher f, supporting a different scaling behavior. In this region the transition from rigid rods to flexible chains sets in.

The change in the scattering behavior can be correlated to the persistence length, $l_p \sim 1.9/q^*$,[42] where q^* is the scattering vector value at which the scaling law behavior changes. WLM persistence length values obtained from fitting the SLS data according to eqs 3−12 are reported in the inset of Figure 9 together with data obtained from microscopy measurements. The trend of the persistence length normalized by the interfacial tension as a function of micelle diameter is reported in Figure 9: a d^4 stiffness scaling relation better describes the trend indicating more solid objects.

DISCUSSION

The goal of this paper was to establish a link between the morphology of self-assembled block copolymer systems and

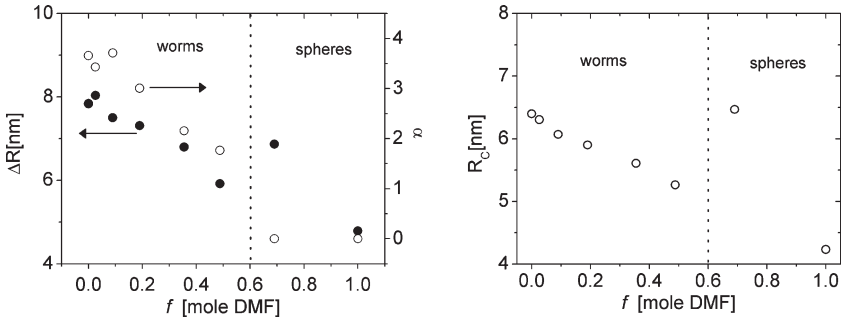

Figure 7. (a) Shell thickness (full circle) and the exponent α (open circle) and (b) core radius as a function of DMF content.

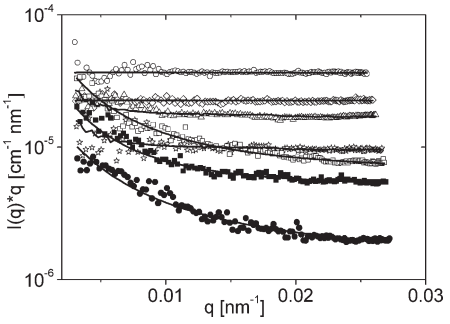

Figure 8. Holtzer plot representation of the light scattering data for different water/DMF mixtures (open circle for $f = 0$, diamond for $f = 0.06$, triangle for $f = 0.09$, star for $f = 0.2$, open square for $f = 0.26$, full square for $f = 0.35$, full circle for $f = 0.6$).

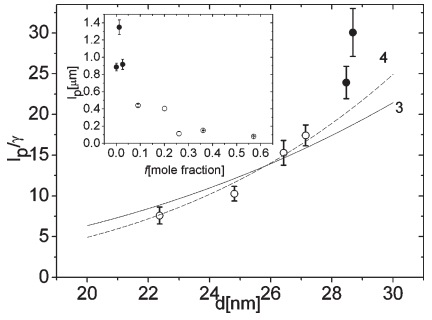

Figure 9. Persistence length normalized by the interfacial tension as a function of micelle diameter. Key: full circle, microscopy data; open circle, light scattering data. Lines: $l_p/\gamma \sim d^n$ with $n = 3$ (straight line) and $n = 4$ (dashed line). Inset: Persistence length as a function of the DMF mole fraction.

the internal structure of these systems, while changing the solvent selectivity of the block copolymer by varying the molar ratio of mixtures of DMF and water. The obvious morphological changes are that with increasing DMF molar fraction f, the contour length (see Figure 3) as well as the persistence length (see insert Figure 9) become shorter, resulting finally in a morphological transition from worm-like to spherical micelles . As a consequence the mean total aggregation number almost halved going from pure water to $f = 0.026$ (see Table 2).

This is a unique result, which could only be obtained by combining SANS with light microscopy and scattering and can be interpreted as a consequence of the change in the solvent selectivity while DMF is added to the solution.

Table 2. Samples' Solvent Composition Expressed as DMF Mole Fraction (f); Interfacial Tension, γ; the Aggregation Number per Unit Length in the Case of Wormlike Micelles, n_{agg}; the Area per Chain at the Interface, a_{chain}; the Stretching of the Core Chains, S_C; the Tethering Density, $\tilde{\sigma}$; the Mean Total Micellar Aggregation Number, N_{tot}[b]

f		γ [mN m^{-1}]	n_{agg}	a_{chain} [nm^2]	S_C	$\tilde{\sigma}$	N_{tot}[a]
0	w	37.2	27	1.61	1.52	9.6	34 573
0.026	w	30.6	26	1.64	1.50	9.4	22 338
0.09	w	25.3	24	1.69	1.45	9.1	
0.2	w	20	23	1.75	1.40	8.8	
0.36	w	14.7	21	1.84	1.33	8.4	
0.5	w	10.6	18	1.94	1.26	7.9	
0.7	s	8.2		2.38	1.55	6.5	223
1	s	5.3		3.68	1.00	4.2	68

[a] For the samples between $f = 0.09$ and 0.5 we do not give values for N_{tot} as we do not have a good length determination. [b] w stands for WLM and s for spherical micelles. $l_{PEO} = 0.4$ nm; $l_{PB} = 0.48$ nm; $C_F = 0.68$; $C_H = 1.38$; $l_k = 1.1$ nm; $A_{2,water} = 3.8 \times 10^{-3}$ cm^3 mol/g^2; $A_{2,DMF} = 2.9 \times 10^{-3}$ cm^3 mol/g^2

The morphology adopted by the aggregates depends on a fine balance between the contributions to the free energy of the core, the surface free energy per chain and the corona[3,12−14] is

$$F_{TOT} = F_{core} + F_{int} + F_{shell} \quad (30)$$

The core free energy F_{core} mostly depends on the degree of stretching of PB chains in the core, S_c;

$$\frac{F_{core}}{kT} = \beta S_C^2 \quad (31)$$

where β is equal to $\pi^2/16$ in the case of cylinders and $3\pi^2/80$ for spheres.[43] The surface free energy F_{int} depends on the core/corona interfacial tension γ and the area per chain at the interface, a_{chain}:

$$F_{int} = \gamma a_{chain} \quad (32)$$

The corona free energy per chain is a balance between elastic stretching and repulsions of the chains.[44] Assuming the scaling exponent 3/5 for good solvent it is given by[12]

$$\frac{F_{shell,cyl}}{kT} = \sqrt{2}\widehat{C}_F r^{3/2} N_{PB}^{-1/2} \left\{ \left[1 + \frac{\sqrt[3]{2^5}}{3} \left(\frac{l_{PEO}}{l_{PB}} \right)^{5/3} \widehat{C}_H N_{PEO} r^{-2/3} N_{PB}^{-1/3} \right] \right\}^{3/8} \quad (33)$$

dx.doi.org/10.1021/ma102624b |Macromolecules 2011, 44, 3583–3593

and

$$\frac{F_{shell,sph}}{kT} = \frac{\sqrt{3}}{5}\hat{C}_F r^{3/2} N_{PB}^{-1/2} \times \ln\left[1 + \frac{5}{\sqrt[3]{3^4}}\left(\frac{l_{PEO}}{l_{PB}}\right)^{5/3} \hat{C}_H N_{PEO} r^{-2/3} N_{PB}^{-1/3}\right]^{3/8} \quad (34)$$

for very long cylinders and spherical micelles, respectively.

$r = R_c/l_{PB}$ is the dimensionless radius of the core; l_{PEO} and l_{PB} are the PEO and PB monomer lengths. They are derived from the monomer volume: $l = V_o^{1/3} = (M_o/\rho_{bulk}N_A)^{1/3} = 0.40$ and 0.48 nm for PEO and PB respectively. $\hat{C}_H$ and $\hat{C}_F$ are numerical factors: $\hat{C}_H = C_H(l_k/l_{PEO})^{1/3}v^{1/3}$ and $\hat{C}_F = C_F$, with C_F and C_H model parameters equal to 0.68 and 1.38 according to Zhulina et al.[12] The Kuhn length of the PEO block, l_k, is 1.1 nm according to Rubistein et al.[45] v is the excluded volume parameter:

$$v = 2A_2M_o^2/l_{PEO}^3 N_A \quad (35)$$

with A_2 second virial coefficient, M_o the PEO monomer molecular weight and N_A the Avogadro number. The second virial coefficients for PEO are 3.8×10^{-3} cm^3 mol/g^2 and 2.9×10^{-3} cm^3 mol/g^2 in, respectively, water[46] and DMF,[18,47,48] assuming a $M^{-0.2}$ dependence on the polymer molecular weight.

As can be seen from the definitions, one has to consider both spherical and cylindrical geometries in the different contributions. This determines finally the transition from cylindrical to spherical micelles.

All the microscopic parameters necessary to calculate the different energy contributions can be obtained from the SANS experiments. They are the microscopic origin of the observed morphology.

The a_{chain} and S_c can be deduced from the value of the core radius:

$$a_{chain} = \frac{aN_{PB}V_C}{R_C} \quad (36)$$

$$S_C = \frac{R_C}{R_o} \quad (37)$$

N_{PB} and V_C are the degree of polymerization of the PB block and the volume of the PB repeat unit; a is a coefficient equal to 2 for cylinders and to 3 for spheres; R_o is the unperturbed end-to-end distance of a PB chain ($R_0 = 0.082M_{PB}^{0.5} = 4.2$ nm, where M_{PB} is the molecular weight of the PB block[49]). For both eq 36 and 37, a segregated core is assumed.

From the interfacial tension measurements we know how the surface tension γ decreases with increasing f (see Figure 2). A lower surface tension implies that a larger interfacial area per chain, a_{chain}, can be formed. Our results indeed show that the area per chain a_{chain} increases from 1.61 to 3.68 nm^2 with increasing f, resulting in a decrease of the stretching parameter S_c from to 1.52 to 1.00 (see Table 2).

This effect is probably hampered by the concomitant drop in solvent quality for PEO resulting in shrinkage of the micellar corona (see Figure 7a). This shrinkage is consistent with a lower solvent penetration into the shell as observed by the α parameter values in the fit of the SANS data. The same trend has been observed by Lund et al.[18] on PEPPEO star-like micelles. In the same paper they found a decrease in the second virial coefficient of a PEO homopolymer in different DMF/water mixtures, which nevertheless remain good solvents. At the same time the R_g of the PEO homopolymer was not affected by solvent quality and its values agree well with those predicted by Devanand and Selser scaling law.[46] They attributed this effect to more effective excluded volume interactions in the micellar corona.

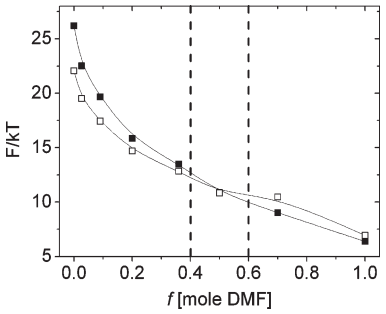

Figure 10. Total (=core + interface + shell) free energy per chain as a function of DMF content in the solvent calculated for the two geometries (full square for spheres and open square for long cylinders). The dashed lines indicate the region where coexistence between spherical and cylindrical micelles could exist.

The area per chain at the interface influences the tethering density at the core−shell interface,

$$\tilde{\sigma} = \pi R_g^2/a_{chain} \quad (38)$$

where R_g is the radius of gyration of PEO chains ($R_g = 0.215M_w^{0.583}$Å = 2.12 nm)[46]

The continuous decrease in $\tilde{\sigma}$ with increasing f, as listed in Table 2, shows that the increase in the a_{chain} can allow for the shrinkage of the PEO corona. $\tilde{\sigma}$ stays always above 3.7, indicating that PEO chains are in the overcrowded regime for both spheres and cylinders, though the PEO chains are approaching the noninteracting regime once they are spherical.[50]

Intuitively these results nicely show that when there is more space in the shell, then it is also easier to bend the cylinder, resulting in a smaller persistence length, as is experimentally observed (see insert in Figure 9).

Finally, if we want to account for the presence of the hemispherical end-caps, as a first approximation the total free energy can be written as

$$F_{TOT,worm} = xF_{TOT,sph} + (1-x)F_{TOT,cyl} \quad (39)$$

where $x = (4\pi R_C^3)/(3N_{PB}V_CN_{TOT})$ is the fraction of PB−PEO molecules in the end-caps. For the samples between $f = 0.09$ and 0.5 we do not have an estimate of $N_{tot} = n_{ag}L$, so we calculated an upper value for x assuming a minimum contour length equal to 500 nm, the maximum length detectable by the light scattering measurements we performed.

The sums of all the free energy contributions calculated according to eq 30−36 and 39 using the microscopic input listed in Table 2 are plotted in Figure 10 for the two geometries.

The most important contribution comes from the core−corona interface which is always higher in the case of spheres. The total micellar free energy for wormlike micelles is lower than that for spherical micelles up to a DMF molar fraction $f = 0.5$, where the two values are very close to each other. At higher DMF concentrations the morphological transition from worm-like micelles to spheres is energetically favored. The energy profile is however continuous, without abrupt change from one morphology to the other. A coexistence region, not detectable with scattering experiments, could exist between $f = 0.4$ and 0.6 where

dx.doi.org/10.1021/ma102624b |Macromolecules 2011, 44, 3583–3593

the energy difference between spherical and cylindrical micelles is less than 5%.

Besides, from our results we can exclude the presence of short cylindrical micelles. They would exist between $f = 0.6$, where SLS experiments show the presence of wormlike micelles, and 0.7, where SANS curve is typical for spheres. As in this range the spherical geometry is already energetically favored, this corroborates the absence of short cylindrical micelles.

CONCLUSIONS

We have studied the behavior of PBPEO wormlike micelles in different water/DMF solvent mixtures. We used different complementary experiments in order to access the micellar structure at different length scales: (i) a combination of fluorescence microscopy and dynamic light scattering worked at low DMF content and showed a decrease of the micellar contour length, (ii) small angle neutron scattering informed us about the local micellar structural parameters, like the rods core and shell diameters, and (iii) static light scattering about the persistence length. With the input of all these results, including also the interfacial tension of PB, we were able to identify all contributions to the micellar free energy of the system, which decreases continuously during the morphological transition from WLM to spheres. The main energy contributions come from the micellar shell and interface indicating that the interfacial tension and the area at the interface are the more important driving parameters. We confirm experimentally that the morphological change from wormlike micelles to spheres takes place at DMF mole fraction between 0.5 and 0.7. With these results, a priori tuning of the system properties is now feasible.

AUTHOR INFORMATION

Corresponding Author

*E-mail: lonetti@chimie.ups-tlse.fr.

Present Addresses

[§]Laboratoire des Interactions Moléculaires et Réactivité Chimique et Photochimique, Université de Toulouse; UPS/CNRS; 118 route de Narbonne, F-31062 Toulouse, Cedex 9, France.

ACKNOWLEDGMENT

A.T. thanks the International Helmholtz Research School BioSoft for financial support. We acknowledge the DFG for financial support within the SFB TR-6.

REFERENCES

(1) Antonietti, M.; Förster, S., *Vesicles and Liposomes: A Self-Assembly Principle Beyond Lipids*; WILEY-VCH Verlag: Weinheim, Germany, 2003; Vol. 15, pp 1323−1333.

(2) Forster, S.; Zisenis, M.; Wenz, E.; Antonietti, M. *J. Chem. Phys.* **1996**, *104* (24), 9956–9970.

(3) Hamley, I. *Block copolymers in solution: fundamentals and applications.*; Wiley: Hoboken, NJ; San Francisco, CA; and Weinheim, Germany,2005.

(4) Smart, T.; Lomas, H.; Massignani, M.; Flores-Merino, M. V.; Perez, L. R.; Battaglia, G. *Nano Today* **2008**, *3* (3−4), 38–46.

(5) Alexandridis, P.; Spontak, R. J. *Curr. Opin. Colloid Interface Sci.* **1999**, *4* (2), 130–139.

(6) Won, Y. Y.; Davis, H. T.; Bates, F. S. *Science* **1999**, *283* (5404), 960–963.

(7) Won, Y. Y.; Brannan, A. K.; Davis, H. T.; Bates, F. S. *J. Phys. Chem. B* **2002**, *106* (13), 3354–3364.

(8) Dalhaimer, P.; Bermudez, H.; Discher, D. E. *J. Polym. Sci., Part B: Polym. Phys.* **2004**, *42* (1), 168–176.

(9) Forster, S.; Berton, B.; Hentze, H. P.; Kramer, E.; Antonietti, M.; Lindner, P. *Macromolecules* **2001**, *34* (13), 4610–4623.

(10) Halperin, A. *Macromolecules* **1987**, *20* (11), 2943–2946.

(11) Izzo, D.; Marques, C. M. *Macromolecules* **1997**, *30* (21), 6544–6549.

(12) Zhulina, E. B.; Adam, M.; LaRue, I.; Sheiko, S. S.; Rubinstein, M. *Macromolecules* **2005**, *38* (12), 5330–5351.

(13) Bang, J.; Jain, S.; Li, Z.; Lodge, T. P.; Pedersen, J. S.; Kesselman, E.; Talmon, Y. *Macromolecules* **2006**, *39* (3), 1199–1208.

(14) Bhargava, P.; Zheng, J. X.; Li, P.; Quirk, R. P.; Harris, F. W.; Cheng, S. Z. D. *Macromolecules* **2006**, *39* (14), 4880–4888.

(15) Denkova, A. G.; Mendes, E.; Coppens, M. O. *J. Phys. Chem. B* **2008**, *112* (3), 793–801.

(16) Shen, H.; Eisenberg, A. *J. Phys. Chem. B* **1999**, *103* (44), 9473–9487.

(17) Liang, Y. Z.; Li, Z. C.; Li, F. M. *Chem. Lett.* **2000**, No. 4, 320–321.

(18) Lund, R.; Willner, L.; Stellbrink, J.; Radulescu, A.; Richter, D. *Macromolecules* **2004**, *37* (26), 9984–9993.

(19) Choucair, A.; Eisenberg, A. *Eur. Phys. J. E: Soft Matter Biol. Phys.* **2003**, *10* (1), 37–44.

(20) Denkova, A. G.; Mendes, E.; Coppens, M. O. *Soft Matter* **2010**, *6* (11), 2351–2357.

(21) Lonetti, B.; Kohlbrecher, J.; Willner, L.; Dhont, J. K. G.; Lettinga, M. P. *J. Phys.-Condens. Matter* **2008**, *20* (40), 404207.

(22) Allgaier, J.; Poppe, A.; Willner, L.; Richter, D. *Macromolecules* **1997**, *30* (6), 1582–1586.

(23) Brangwynne, C. P.; Koenderink, G. H.; Barry, E.; Dogic, Z.; MacKintosh, F. C.; Weitz, D. A. *Biophys. J.* **2007**, *93* (1), 346–359.

(24) Kohlbrecher, J.; Wagner, W. *J. Appl. Crystallogr.* **2000**, *33* (3−1), 804–806.

(25) Choi, S. M.; Barker, J.; Glinka, C.; Cheng, Y.; Gammel, P. *J. Appl. Crystallogr.* **2000**, *33* (3−1), 793–796.

(26) Eskildsen, M. R.; Gammel, P. L.; Isaacs, E. D.; Detlefs, C.; Mortensen, K.; Bishop, D. J. *Nature* **1998**, *391* (6667), 563–566.

(27) Pedersen, J. S. Modelling of Small Angle Sacttering Data from Colloids and Polymer Systems. In *Neutrons, X-Ray and Light*, Lindner, P., Zemb, T., Eds.; Elsevier Science: Amsterdam, 2002.

(28) Borsali, R.; Percora, R., *Soft Matter Characterization*. Springer: Berlin, 2008; p 208.

(29) Kholodenko, A. L. *Macromolecules* **1993**, *26* (16), 4179–4183.

(30) http://kur.web.psi.ch/sans1/SANSSoft/sasfit.html

(31) Pedersen, J. S. *Adv. Colloid Interface Sci.* **1997**, *70*, 171–210.

(32) Dhont, J. K. G. *Studies in Interface Science*. Elsevier: 1996; Vol. II, An Introduction to Dynamics of Colloids.

(33) Ortega, A.; Garcia de la Torre, J. *J. Chem. Phys.* **2003**, *119*, 9914–9919.

(34) Dalhaimer, P.; Bates, F. S.; Discher, D. E. *Macromolecules* **2003**, *36* (18), 6873–6877.

(35) Song, L.; Kim, U. S.; Wilcoxon, J.; Schurr, J. M. *Biopolymers* **1991**, *31* (5), 547–567.

(36) Helfand, E.; Tagami, Y. *J. Polym. Sci., Part B: Polym. Lett.* **1971**, *9* (10), 741–746.

(37) Sato, T.; Teramoto, A. *Adv. Polym. Sci.* **1996**, *126*, 85–161.

(38) Sato, T.; Takada, Y.; Teramoto, A. *Macromolecules* **1991**, *24* (23), 6220–6226.

(39) Sato, T.; Einaga, Y. *Langmuir* **2007**, *24* (1), 57–61.

(40) Einaga, Y. *Polym. J.* **2009**, *41* (3), 157–173.

(41) Won, Y. Y.; Davis, H. T.; Bates, F. S.; Agamalian, M.; Wignall, G. D. *J. Phys. Chem. B* **2000**, *104* (30), 7134–7143.

(42) Marignan, J.; Appell, J.; Bassereau, P.; Porte, G.; May, R. P. *J. Phys.* **1989**, *50* (24), 3553–3566.

(43) Lairez, D.; Adam, M.; Carton, J. P.; Raspaud, E. *Macromolecules* **1997**, *30* (22), 6798–6809.

(44) Halperin, A.; Tirrell, M.; Lodge, T. P. *Adv. Polym. Sci.* **1992**, *100*, 31–71.
(45) Rubinstein, M.; Colby, R. H. *Polymer Physics*; Oxford University Press: New York, 2003.
(46) Devanand, K.; Selser, J. C. *Macromolecules* **1991**, *24* (22), 5943–5947.
(47) Duval, M.; Sarazin, D. *Polymer* **2000**, *41* (7), 2711–2716.
(48) Brandrup, J.; Immergut, E. H., *Polymer Handbook VII/132*; Wiley Interscience: New York, 1989.
(49) Brandrup, J.; Immergut, E. H., *Polymer Handbook VII/33*; Wiley Interscience: New York, 1989.
(50) Zheng, J. X.; Xiong, H.; Chen, W. Y.; Lee, K.; Van Horn, R. M.; Quirk, R. P.; Lotz, B.; Thomas, E. L.; Shi, A.-C.; Cheng, S. Z. D. *Macromolecules* **2005**, *39* (2), 641–650.